Optimized CGenFF force-field parameters for acylphosphate and N-phosphonosulfonimidoyl functional groups

Lamees Hegazy[§] and **Nigel G. J. Richards**[‡,*]

[§]Department of Chemistry, University of Florida, Gainesville, FL 32611, USA

[‡]Department of Chemistry & Chemical Biology, Indiana University Purdue University Indianapolis, Indianapolis, IN 46202, USA

Abstract

We report an optimized set of CGenFF parameters that can be used to model small molecules containing acylphosphate and N-phosphonosulfonimidoyl functional groups in combination with the CHARMM force field. Standard CGenFF procedures were followed to obtain bonded interaction parameters, which were validated by geometry optimizations, comparison to the results of calculations at the MP2/6-31+G(d) level of theory, and molecular dynamics simulations. In addition, partial atomic charges were assigned so that the energy of hydrogen bonding of the model compounds with water was correctly reproduced. The availability of these parameters will facilitate computational studies of enzymes that generate acyladenylate intermediates during catalytic turnover. In addition, given that the N-phosphonosulfonimidoyl moiety is a stable transition state analog for the reaction of ammonia with an acyladenylate, the parameters developed in this study should find use in efforts to develop novel and potent inhibitors of various glutamine-dependent amidotransferases that have been validated as drug targets. Topology and parameter files for the model compounds used in this study, which can be combined with other CGenFF parameters in computational studies of more complicated acylphosphates and N-phosphonosulfonimidates are made available.

Keywords

CGenFF; Parameters; Acylphosphates; Sulfoximines; N-Phosphonosulfonimidates; Force Field; Drug Discovery

Introduction

A significant number of metabolic enzymes activate substrates for reaction by adenylation [1], including validated drug targets such as tRNA aminoacyl synthetases [2], glutamine-dependent NAD$^+$ synthetase [3, 4] and aminoacyl-tRNA transamidating enzymes [5–7] (Fig. 1). In addition, recent studies have identified glutamine-dependent asparagine synthetase (ASNS) [8] (Fig. 1) as (i) a critical component in the development of prostate cancer [9], and (ii) a biomarker for ovarian cancer [10]. Although its precise physiological role remains hotly debated, ASNS has also been implicated in the molecular mechanisms underlying the onset of drug-resistant acute lymphoblastic leukemia [8, 11, 12]. ASNS inhibitors therefore

[*]Corresponding author: Nigel Richards. ngrichar@iupui.edu. Tel: +1 317 274 6624.

have clinical potential for use in the treatment of leukemia and solid tumors, such as those of the prostate and ovary. Our group has reported that functionalized sulfoximines, such as **1** and **2** (Fig. 2), are the first small molecule inhibitors of human ASNS with nanomolar potency, and has established that these compounds can kill, or suppress, the proliferation of asparaginase-resistant MOLT-4 cells [13, 14]. Structure-based identification of sulfoximine derivatives that are more "druglike" [15, 16], and therefore possess improved cell permeability and bioactivity, using computational methods is precluded, however, by a lack of force field parameters that describe the N-phosphonosulfonimidoyl moiety. Similarly, efforts to obtain optimized structures of ASNS complexed to acyladenylates, such as **3**, which are needed for virtual screening studies [17] are hampered by an absence of parameters for acylphosphates. We now report optimized parameters for both the acylphosphate and N-phosphonosulfonimidoyl functional groups, which have been obtained following the systematic procedures used to develop the CHARMM General Force Field (CGenFF) [18]. As a result, these parameters are compatible with the CHARMM all-atom additive force field used to simulate biological molecules [19, 20]. Our parameter values should also facilitate efforts to (i) obtain a detailed understanding of enzymes that catalyze acyladenylate formation and (ii) identify novel small molecules with potential clinical application as anti-cancer and antibacterial agents.

Computational Methods

Calculations to obtain the missing parameters needed to describe the conformational and intermolecular energetics of functionalized acylphosphates and N-phosphorylated sulfoximines were performed on the model compounds **4** and **5** (Fig. 3). Initial guesses were obtained from the ParamChem web site (www.paramchem.org) using automated algorithms [21, 22]. The global energy minima for **4** and **5** were identified at the MP2/6-31+G(d) level of theory [23, 24], as implemented in Gaussian09 [25], by geometry optimization (default tolerances). Standard CGenFF Lennard-Jones parameters were used for all atoms, and an initial set of atomic partial charges was assigned by analogy to those of similar CGenFF atom types using ParamChem. Vibrational spectra were calculated for the optimized geometries of **4** and **5** to (i) ensure that these structures did represent energy minima, and (ii) obtain frequencies and their assignments to specific modes. The numerical values of all QM frequencies were scaled by 0.943 prior to comparison with those calculated using empirical potential energy functions [26]. As described elsewhere [18], water molecules in the TIP3P geometry [27] were placed around **4** and **5** so as to form hydrogen bonding interactions with all donor/acceptor groups (Fig. 4), and each model/water interaction distance was optimized at the HF/6-31G(d) level [28, 29] with the remaining degrees of freedom fixed. We note that both tetrahedral ("lone pair") and trigonal hydrogen bonding interactions between water and oxygen atoms (R-O-R` and terminal oxygen atoms) were considered, and partial charges assigned in order to obtain the best agreement between the interaction energies for all orientations.

All empirical force field calculations were performed using the program CHARMM version 35 [30], which allowed us to define new atom types with names of up to six characters. An RMS gradient of 10^{-5} kcal/mol/Å was employed in energy minimizations and subsequent vibrational analyses were performed using the VIBRAN and MOLVIB modules in CHARMM. No non-bonded interaction distance cutoffs were used in these calculations.

A potential energy scan (PES) for each selected dihedral angle was calculated, in 15° increments, using the scan facility (keyword: "Opt = ModRedundant") implemented within Gaussian09 [25], with structures being optimized at the MP2/6-31+G(d) level. Single point energies were subsequently determined for each structure at its optimized geometry using MP2/cc-pVTZ calculations. The corresponding PES calculated using the CHARMM

empirical energy function employed the QM geometries as initial guesses, each structure being energy minimized with the dihedral angle of interest being restrained with a harmonic potential (force constant of 10^4 kcal/mol/rad). The harmonic restraints were not removed prior calculating conformational energies.

Each model compound **4** and **5** was solvated in octahedral box (28 Å × 28 Å × 28 Å) of TIP3P water molecules [27] and energy minimized by steepest descent (SD) and adopted basis Newton-Raphson (ABNR) algorithms [30]. Periodic boundaries were used in all MD simulations with the particle mesh Ewald method [31] being used to obtain electrostatic energies. Equations of motion were integrated over 1 fs time steps, with covalent bonds to hydrogen being constrained using the SHAKE algorithm [32]. After heating to 300 K (30 ps), each system was equilibrated for a further 40 ps in the NVT ensemble before the "production" MD simulation was performed in the NPT ensemble (2 ns). Constant temperature and pressure (1 atm) were achieved by coupling the systems to a Langevin thermostat and a Nosé–Hoover Langevin barostat, respectively [33, 34].

Missing loops in the X-ray crystal structure of γ-glutamylcysteine synthetase complexed with the N-phosphorylated sulfoximine **6** (Fig. 2) (1VA6) [35] were modeled using the CHIMERA interface to MODELLER [36, 37]. The resulting model complex was then solvated in octahedral box (87 Å × 87 Å × 87 Å) of TIP3P water molecules [27] and energy minimized by steepest descent (SD) and adopted basis Newton-Raphson (ABNR) algorithms so that the final structure possessed an RMS gradient of 10^{-5} kcal/mol/Å [30]. Periodic boundaries were used in this calculation with the particle mesh Ewald method [31] being used to obtain electrostatic energies.

Results and discussion

Parameterization

In order to ensure compatibility with the existing CHARMM force field for proteins and nucleic acids [19, 20], standard protocols [18] were used to generate missing parameters for bonds and bond angles in the model acylphosphate **4** and the N-phosphonosulfonimidoyl derivative **5** (Fig. 3). Thus, the lowest energy conformations for these two molecules were located by standard search procedures, and geometry optimization was carried out at the MP2/6-31+G(d) level given that both are mono-anions. Vibrational frequency analysis confirmed that these structures were true energy minima.

Water molecules were positioned about each of the lowest energy structures so as to make idealized hydrogen bonding interactions, and then atomic partial charges were optimized to give the best agreement between the non-covalent interaction energies and bond distances calculated using HF/6-31G(d) and CGenFF (Table 2). In this procedure, each molecule-water complex was built by optimizing the hydrogen bond distance between each model compound, at its MP2/6-31G(d) optimized geometry, and a TIP3P water while fixing all other degrees of freedom. Although a higher level of theory would have given more accurate results, QM calculations were performed with HF/6-31G(d) in order to be consistent with the methodology used to develop the CHARMM force field for biological molecules. The choice of optimized partial atomic charges was constrained by (i) requiring that the value on all hydrogen atoms was 0.09, (ii) maintaining the initial set of CGenFF charges on carbons C4 and in C11 in acylphosphate **4** and on carbons C4, C9 and C11 in N-phosphonosulfonimidoyl derivative **5**, and (iii) the summation of all atomic charges to −1 (Table 1). After partial charge optimization, all CGenFF energies were within 0.2 kcal/mol of the corresponding HF/6-31G(d) value and the CGenFF distances were 0.2 Å shorter than those computed quantum mechanically (Table 2).

Having established good parameters for calculating non-bonded interaction energies, we optimized the reference values for the bond lengths, bond and dihedral angles, and improper torsions. Force constants were adjusted so that the MOLVIB vibrational frequencies, together with contributions of different harmonic modes to each vibration, were in good agreement with MP2/6-31G(d) values that had been scaled by 0.943. Manual adjustment of the force constants then gave optimized CGenFF structures for **4** and **5** that were in excellent agreement with those calculated at the MP2/6-31+G(d) level of theory (Table 3), i.e. CGenFF-optimized structures had bond lengths and angles within 0.03 Å and 3° of the QM-derived values, respectively [18].

With optimized partial atomic charges and parameters for bonds and bond angles in hand, we adjusted the amplitudes, multiplicities and phases for the new dihedral angle interactions (Table 4 and Table S1 in supporting information). Thus, amplitudes for missing dihedrals composed only of non-hydrogen atoms were chosen so as to reproduce the adiabatic potential energy scans (PES) computed by *ab initio* methods (Fig. 5 and Fig. 6). Although the C4-O3-P1-O8 dihedral for the acylphosphate moiety was not a missing parameter in the CHARMM force-field, efforts to obtain good agreement between the QM and MM potential energy curves for our model compound **4** proved to be difficult. We therefore assigned a new atom type to O8 (Fig. 3), which enabled the development of optimized dihedral potentials for acylphosphate **4** while retaining the original parameterization of the C4-O3-P1-O8 dihedral interaction for modeling nucleic acids. The Lennard-Jones parameters for the OG305 atom type were identical to those of the OG303 atom type. On the other hand, for the O3-P1-O8-C9 dihedral angle (e.g. Fig. 5B) it proved impossible to identify parameters that completely reproduced the complete QM PES including minima and barriers heights. In this case, we therefore sought to maximize agreement between the QM and MM potential energy curves for the low energy regions rather than all the barrier heights.

Parameter validation studies using energy minimization

Our initial effort at parameter validation examined whether the extent to which those for the N-phosphonosulfonimidoyl functional group could reproduce data from X-ray crystal structures. Given the absence of small molecule structures for adenylylated sulfoximines in the Cambridge Structural Database [38] we chose to evaluate the performance of our parameters in modeling the sulfoximine phosphate **6** (Fig. 2) that is bound to the enzyme γ-glutamylcysteine synthetase [35]. After the insertion of missing loops in the X-ray crystal structure (1VA6) using the CHIMERA interface to MODELLER [36, 37], the resulting structure was energy minimized in an octahedral box of TIP3P water molecules [27]. Superimposition of the energy minimized structure of **6** with that in the original X-ray crystal structure showed good agreement between the optimized and experimental bond lengths and bond angles (Fig. 7).

Parameter validation studies using molecular dynamics simulations

As a further validation of the new CGenFF parameters obtained using model compounds **4** and **5**, we performed molecular dynamics (MD) simulations of these two small molecules in aqueous solution. Over a period of 16 ns, rotation of the phosphate group was observed (Fig 8 and Fig S1 in supporting information), and no major bond length or bond angle distortions occurred during the simulation. In addition, the torsion angles for which new parameters had been developed (Tables 5 and 6) fluctuated about values corresponding to minima on the potential energy surface (Figs 5 and 6). This data therefore suggests that these CGenFF parameters will be suitable for use in the simulated annealing [39], *in silico* docking [40] and free energy perturbation calculations [41] that will be undertaken as part of future drug discovery efforts.

Summary

We have developed the first optimized set of CGenFF parameters for acylphosphates and N-phosphonosulfonimidates. Although we employed the recommended protocol for obtaining small molecule parameters that are consistent with the CHARMM force field, these values should also represent a useful starting point for the development of alternate sets of optimized parameters for acylphosphate and N-phosphonosulfonimidoyl functional groups for use with the AMBER [42] or GROMOS [43] force fields. More importantly, our results should be generally useful to medicinal chemists seeking to discover potent inhibitors of a variety of enzymes, including glutamine synthetase [44], HIV-1 protease [45], γ-glutamylcysteine synthetase [35,46], and *Leishmania* typanothione synthetase-amidase [47]. In the case of human ASNS, access to these parameters will also facilitate our efforts to use free energy perturbation methods to (i) delineate which diastereoisomer of **1** and **2** binds most tightly to the enzyme [13, 14], and (ii) examine the ability of novel sulfoximine derivatives to act as potent ASNS inhibitors. These calculations will be reported in due course.

Supplementary Material

Refer to Web version on PubMed Central for supplementary material.

Acknowledgments

References

1. Frey, PA.; Hegeman, AD. Enzymatic reaction mechanisms. Oxford: Oxford University Press; 2007.

2. Agarwal V, Nair SK. Aminoacyl tRNA synthetases as targets for antibacterial development. Med Chem Commun. 2012; 3:887–898.

3. LaRonde-LeBlanc N, Resto M, Gerratana B. Regulation of active site coupling in glutamine-dependent NAD+ synthetase. Nat Struct Mol Biol. 2009; 16:421–429. [PubMed: 19270703]

4. Duckworth BP, Nelson KM, Aldrich CC. Curr Topics Med Chem. 2012; 12:766–796.

5. Curnow AW, Hong KW, Yuan R, Kim SI, Martins O, Winkler W, Henkin TM, Soll D. GlutRNA(Gln) amidotransferase: A novel heterotrimeric enzyme required for correct decoding of glutamine codons during translation. Proc Natl Acad Sci, USA. 1997; 94:11819–11826. [PubMed: 9342321]

6. Horiuchi KY, Harpel MR, Shen L, Luo Y, Rogers KC, Copeland RA. Mechanistic studies of reaction coupling in Glu-tRNA(Gln) amidotransferase. Biochemistry. 2001; 40:6450–6457. [PubMed: 11371208]

7. Oshikane H, Sheppard K, Fukai S, Nakamura Y, Ishitani R, Numata T, Sherrer RI, Feng L, Schmitt E, Panvert M, Blanquet S, Mchulam Y, Soll D, Nureki O. Structural recruitment of glutamine to the genetic code. Science. 2006; 312:1950–1954. [PubMed: 16809540]

8. Richards NGJ, Kilberg MS. Asparagine synthetase chemotherapy. Annu Rev Biochem. 2006; 75:629–654. [PubMed: 16756505]

9. Sircar K, Huang H, Hu LM, Cogdell D, Dhillon J, Tzelepi V, Efstathiou E, Koumakpayi IH, Saad F, Luo DJ, Bismar TA, Aparicio A, Troncoso P, Navone N, Zhang W. Integrative molecular profiling reveals asparagine synthetase is a target in castration-resistant prostate cancer. Am J Pathol. 2012; 180:893–903.

10. Lorenzi PL, Llamas J, Gunsior M, Ozbun L, Reinhold WC, Varma S, Ji H, Kim H, Hutchinson AA, Kohn EC, Goldsmith PK, Birrer MJ, Weinstein JN. Asparagine synthetase is a predictive

biomarker of L-asparaginase activity in ovarian cancer cell lines. Mol Cancer Therapeut. 2008; 7:3123–3128.

11. Aslanian AM, Kilberg MS. Asparagine synthetase expression is sufficient to induce L-asparaginase resistance in MOLT-4 leukemia cells. Biochem J. 2001; 357:321–328. [PubMed: 11415466]

12. Tong WH, Pieters R, Hop WCJ, Lanvers-Kaminsky C, Boos J, van der Sluis IM. No evidence of increased asparagine levels in the bone marrow of patients with acute lymphoblastic leukemia during asparaginase therapy. Ped Blood Canc. 2013; 60:258–261.

13. Ikeuchi H, Ahn Y-M, Otokawa T, Watanabe B, Hegazy L, Hiratake J, Richards NGJ. A sulfoximine-based inhibitor of human asparagine synthetase kills L-asparaginase-resistant leukemia cells. Bioorg Med Chem. 2012; 20:5915–5927. [PubMed: 22951255]

14. Gutierrez JA, Pan Y-X, Koroniak L, Hiratake J, Kilberg MS, Richards NGJ. An inhibitor of human asparagine synthetase suppresses proliferation of an L-asparaginase-resistant leukemia cell line. Chem Biol. 2006; 13:1339–1347. [PubMed: 17185229]

15. Hann MM, Keserü GM. Finding the sweet spot: the role of nature and nuture in medicinal chemistry. Nat Rev Drug Disc. 2012; 11:355–365.

16. Walters WP, Green J, Weiss JR, Murcko MA. What do medicinal chemists actually make? A 50-year retrospective. J Med Chem. 2011; 54:6405–6416. [PubMed: 21755928]

17. Morris GM, Huey R, Lindstrom W, Sanner MF, Belew RK, Goodsell DS, Olson AJ. AutoDock4 and AutoDockTools4: Automated docking with selective receptor flexibility. J Comput Chem. 2009; 30:2785–2791. [PubMed: 19399780]

18. Vanommeslaeghe K, Hatcher E, Acharya C, Kundu S, Zhong S, Shim J, Darian E, Guvench O, Lopes P, Vorobyov I, MacKerell AD Jr. CHARMM general force field: A force field for drug-like molecules compatible with the CHARMM all-atom additive biological force fields. J Comput Chem. 2010; 31:671–690. [PubMed: 19575467]

19. MacKerell AD, Bashford D, Bellott M, et al. All-atom empirical potential for molecular modeling and dynamics studies of proteins. J Phys Chem B. 1998; 102:3586–3616.

20. Foloppe N, MacKerell AD. All-atom empirical force field for nucleic acids: I Parameter optimization based on small molecule and condensed phase macromolecular target data. J Comput Chem. 2000; 21:86–104.

21. Vanommeslaeghe K, MacKerell AD Jr. Automation of the CHARMM general force field (CGenFF) I: Bond perception and atom typing. J Chem Inf Mol Model. 2012; 52:3144–3154.

22. Vanommeslaeghe K, MacKerell AD Jr. Assignment of bonded parameters and partial atomic charges. J Chem Inf Mol Model. 2012; 52:3155–3168.

23. Francl MM, Pietro WJ, Hehre WJ, Binkley JS, Gordon MS, DeFrees DJ, Pople JA. Self-consistent molecular orbital methods. XXIII. A polarization-type basis set for second row elements. J Chem Phys. 1982; 77:3654–3665.

24. Head-Gordon M, Pople JA, Frisch MJ. MP2 energy evaluation by direct methods. Chem Phys Lett. 1988; 153:503–506.

25. Frisch, MJ.; Trucks, GW.; Schlegel, HB.; Scuseria, GE.; Robb, MA.; Cheeseman, JR.; Scalmani, G.; Barone, V.; Mennucci, B.; Petersson, GA.; Nakatsuji, H.; Caricato, M.; Li, X.; Hratchian, HP.; Izmaylov, AF.; Bloino, J.; Zheng, G.; Sonnenberg, JL.; Hada, M.; Ehara, M.; Toyota, K.; Fukuda, R.; Hasegawa, J.; Ishida, M.; Nakajima, T.; Honda, Y.; Kitao, O.; Nakai, H.; Vreven, T.; Montgomery, JA., Jr; Peralta, JE.; Ogliaro, F.; Bearpark, M.; Heyd, JJ.; Brothers, E.; Kudin, KN.; Staroverov, VN.; Kobayashi, R.; Normand, J.; Raghavachari, K.; Rendell, A.; Burant, JC.; Iyengar, SS.; Tomasi, J.; Cossi, M.; Rega, N.; Millam, JM.; Klene, M.; Knox, JE.; Cross, JB.; Bakken, V.; Adamo, C.; Jaramillo, J.; Gomperts, R.; Stratmann, RE.; Yazyev, O.; Austin, AJ.; Cammi, R.; Pomelli, C.; Ochterski, JW.; Martin, RL.; Morokuma, K.; Zakrzewski, VG.; Voth, GA.; Salvador, P.; Dannenberg, JJ.; Dapprich, S.; Daniels, AD.; Farkas, Ö.; Foresman, JB.; Ortiz, JV.; Cioslowski, J.; Fox, DJ. Gaussian 09. Wallingford: Gaussian Inc.; 2009.

26. Scott AP, Radom L. Harmonic vibrational frequencies: An evaluation of Hartree-Fock, Möller-Plesset, quadratic configuration interaction, density functional theory, and semi-empirical scale factors. J Phys Chem. 1996; 100:16502–16513.

27. Jorgensen WL, Chandrasekhar J, Madura JD, Impey RW, Klein ML. Comparison of simple potential functions for simulating liquid water. J Chem Phys. 1983; 79:926–935.

28. Ditchfield R, Hehre WJ, Pople JA. Self-consistent molecular orbital methods. 9. Extended Gaussian-type basis for molecular orbital studies of organic molecules. J Chem Phys. 1971; 54:724–728.

29. Frisch MJ, Pople JA, Binkley JS. Self-consistent molecular orbital methods. 25. Supplementary functions for Gaussian basis sets. J Chem Phys. 1984; 80:3265–3269.

30. Brooks BR, Brooks CL III, MacKerell AD Jr, Nilsson L, Petella RJ, Roux B, Won Y, Archontis G, Bartels C, Boresch S, Caflisch A, Caves L, Cui Q, Dinner AR, Feig M, Fischer S, Gao J, Hodoscek M, Im W, Kuczera K, Lazaridis T, Ma J, Ovchinnikov V, Paci E, Pastor RW, Post CB, Pu JZ, Schaefer M, Tidor B, Venable RM, Woodcock HL, Wu X, Yang W, York DM, Karplus J. CHARMM: The biomolecular simulation program. J Comput Chem. 2009; 30:1545–1614. [PubMed: 19444816]

31. Darden T, York D, Pedersen L. Particle mesh Ewald: An Nlog(N) method for Ewald sums in large systems. J Chem Phys. 1993; 98:10089–10092.

32. Ryckaert JP, Ciccotti G, Berendsen HJC. Numerical integration of Cartesian equations of motion of a system with constraints: Molecular dynamics of n-alkanes. J Comput Phys. 1977; 23:327–341.

33. Tobias DJ, Martyna GJ, Klein ML. Molecular dynamics simulations of a protein in the canonical ensemble. J Phys Chem. 1993; 97:12959–12966.

34. Feller SE, Zhang Y, Pastor RW, Brooks BR. Constant pressure molecular dynamics simulation. The Langevin piston method. J Chem Phys. 1995; 103:4613–4621.

35. Hibi T, Nii H, Nakatsu T, Kimura A, Kato H, Hiratake J, Oda J. Crystal structure of γ-glutamylcysteine synthetase: Insights into the mechanism of catalysis by a key enzyme for glutathione homeostasis. Proc Natl Acad Sci USA. 2004; 101:15052–15057. [PubMed: 15477603]

36. Pettersen EF, Goddard TD, Huang CC, Couch GS, Greenblatt DM, Meng EC, Ferrin TE. UCSF Chimera – a visualization system for exploratory research and analysis. J Comput Chem. 2004; 25:1605–1612. [PubMed: 15264254]

37. Marti-Renom MA, Stuart A, Fiser A, Sánchez R, Melo F, Sali A. Comparative protein structure modeling of genes and genomes. Annu Rev Biophys Biomol Struct. 2000; 29:291–325. [PubMed: 10940251]

38. Allen FH. The Cambridge Structural Database: a quarter of a million structures and rising. Acta Crystallogr. B. 2002; 58:380–388. [PubMed: 12037359]

39. Kirkpatrick S, Gelatt CD Jr, Vecchi MP. Optimization by simulated annealing. Science. 1983; 220:671–680. [PubMed: 17813860]

40. Schneider G. Virtual screening: an endless staircase? Nat Rev Drug Discov. 2010; 9:273–276. [PubMed: 20357802]

41. Gallicchio E, Levy RM. Recent theoretical and computational advances for modeling protein-ligand binding affinities. Adv Prot Chem Struct Biol. 2011; 85:27–80.

42. Wang JM, Wolf RM, Caldwell JW, Kollman PA, Case DA. Development and testing of a general amber force field. J Comput Chem. 2004; 25:1157–1174. [PubMed: 15116359]

43. Christen M, Hunenberger PH, Bakowies D, baron R, Burgi R, Geerke DP, Heinz TN, kastenholz MA, Krautler V, Oostenbrink C, Peter C, Trzesniak D, van Gunsteren WF. The GROMOS software for biomolecular simulation: GROMOS05. J Comput Chem. 2005; 26:1719–1751. [PubMed: 16211540]

44. Nilsson MT, Krajewski WW, Yellagunda S, Prabhumurthy S, Chamarahally GN, Siddamadappa C, Srinivasa BR, Yahiaoui S, Larhed M, Karleén A, Jones TA, Mowbray SL. Structural basis for the inhibition of *Mycobacterium tuberculosis* glutamine synthetase by novel ATP-competitive inhibitors. J Mol Biol. 2009; 393:504–513. [PubMed: 19695264]

45. Lu D, Vince R. Discovery of potent HIV-1 protease inhibitors incorporating sulfoximine functionality. Bioorg Med Chem Lett. 2007; 17:5614–5619. [PubMed: 17822899]

46. Hiratake J, Irie T, Tokutake N, Oda J. Recognition of a cysteine substrate by *E. coli* γ-glutamylcysteine synthetase probed by sulfoximine-based transition-state analogue inhibitors. Biosci Biotechnol Biochem. 2002; 66:1500–1514. [PubMed: 12224634]

47. Fyfe PK, Oza SL, Fairlamb AH, Hunter WN. *Leishmania* trypanothione synthetase-amidase structure reveals a basis for regulation of conflicting synthetic and hydrolytic activities. J Biol Chem. 2008; 283:17672–17680. [PubMed: 18420578]
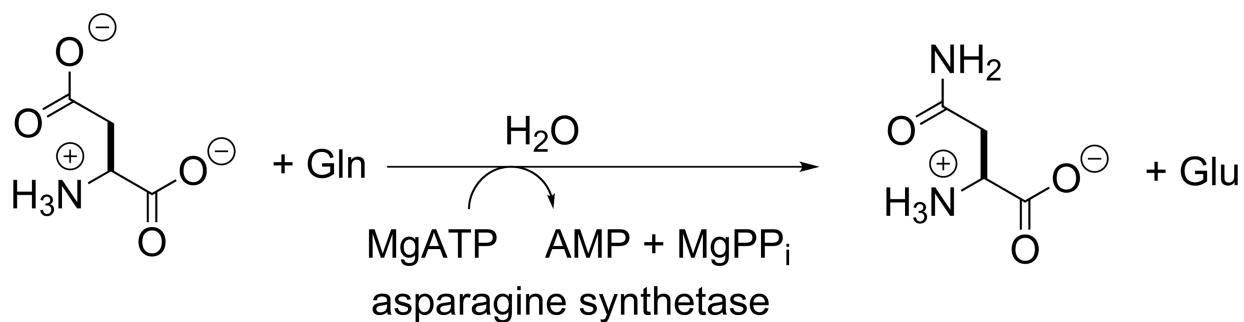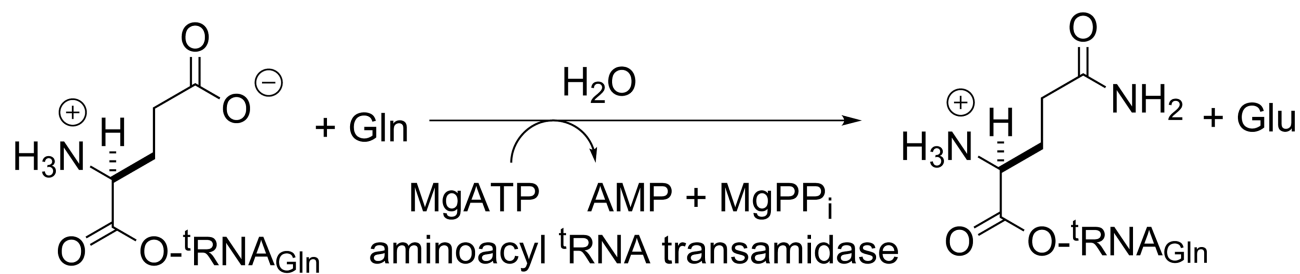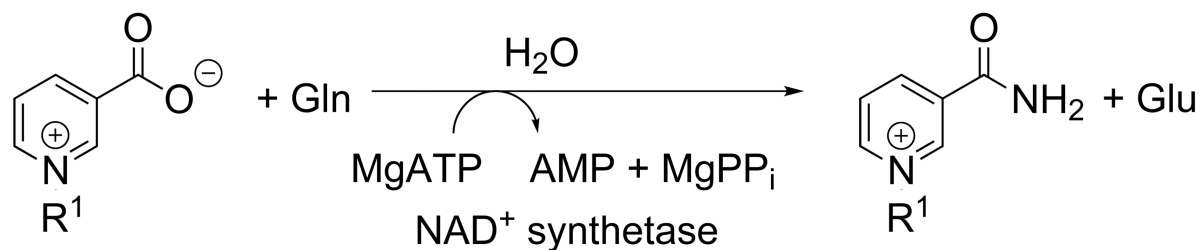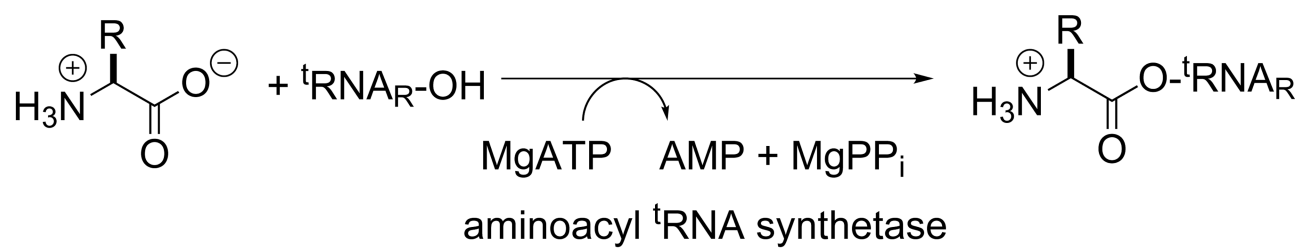
Fig. 1.
Reactions catalyzed by enzymes that activate substrates by adenylylation and are validated drug targets.
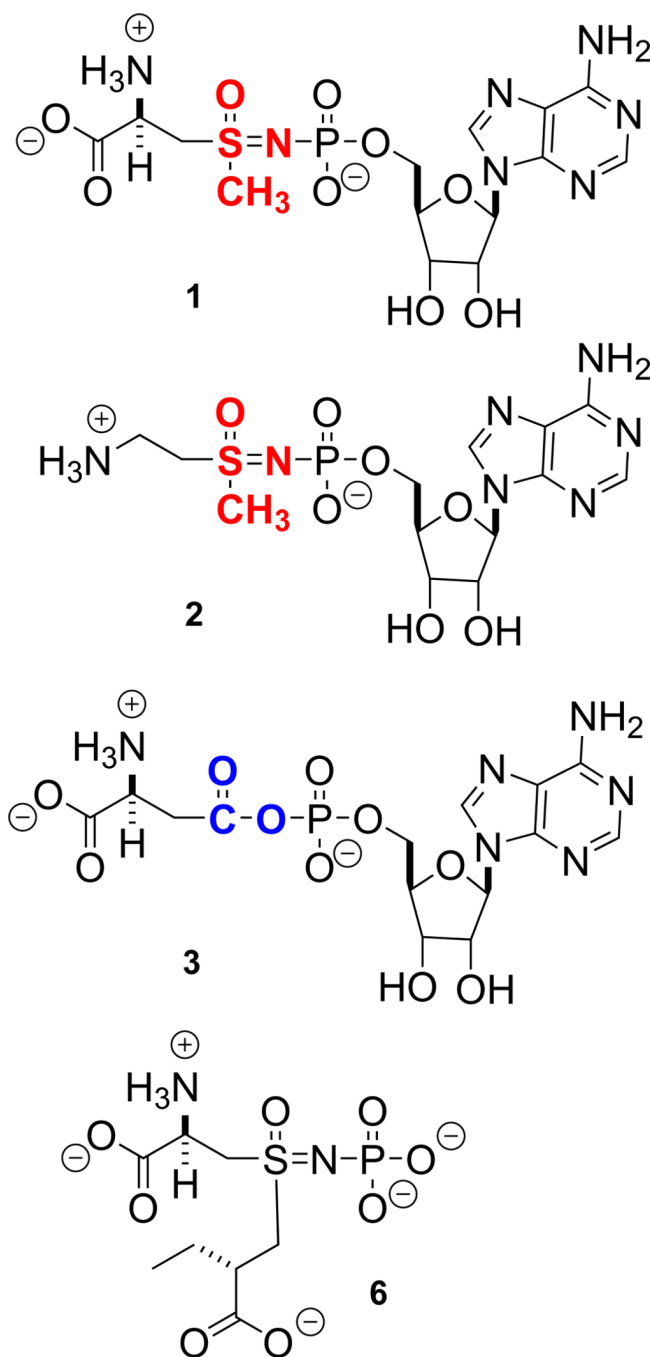
Fig. 2.
Structures of functionalized sulfoximines (**1** and **2**) that are nanomolar inhibitors of human asparagine synthetase (sulfoximine moiety is colored red). These compounds mimic the transition for the reaction of ammonia with the acyladenylate intermediate **3** (acylphosphate moiety highlighted in blue) that is formed during catalytic turnover. Compound **6** is an inhibitor of the enzyme γ-glutamylcysteine synthetase.
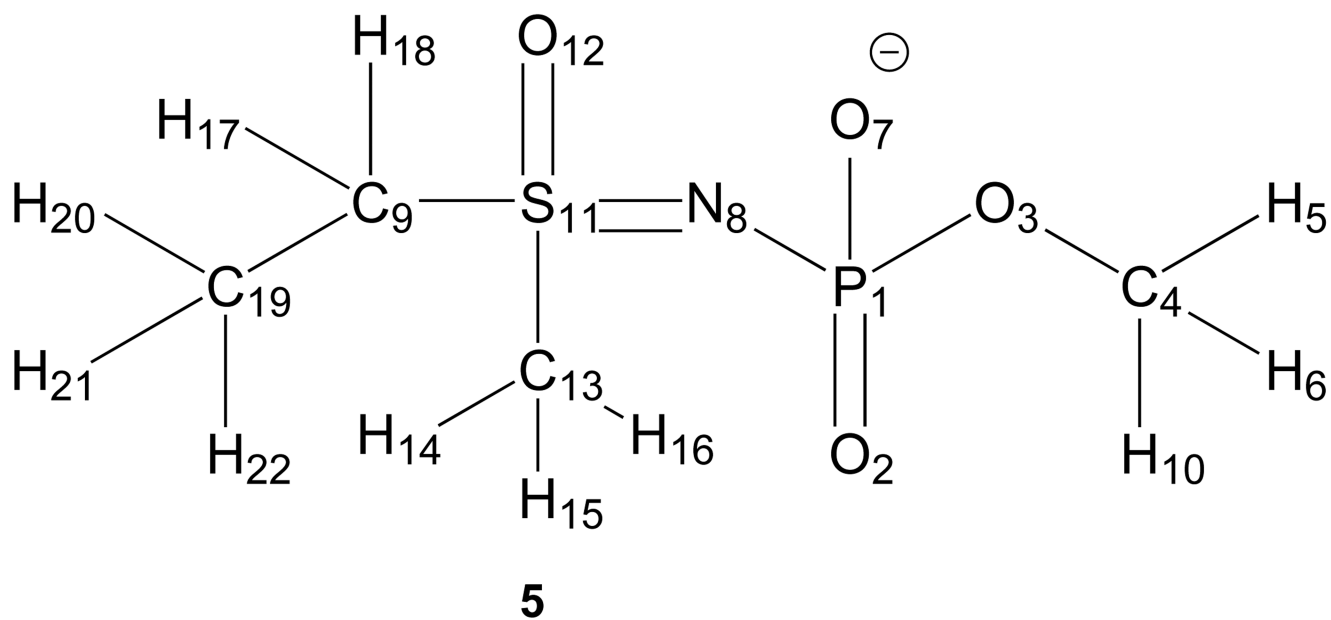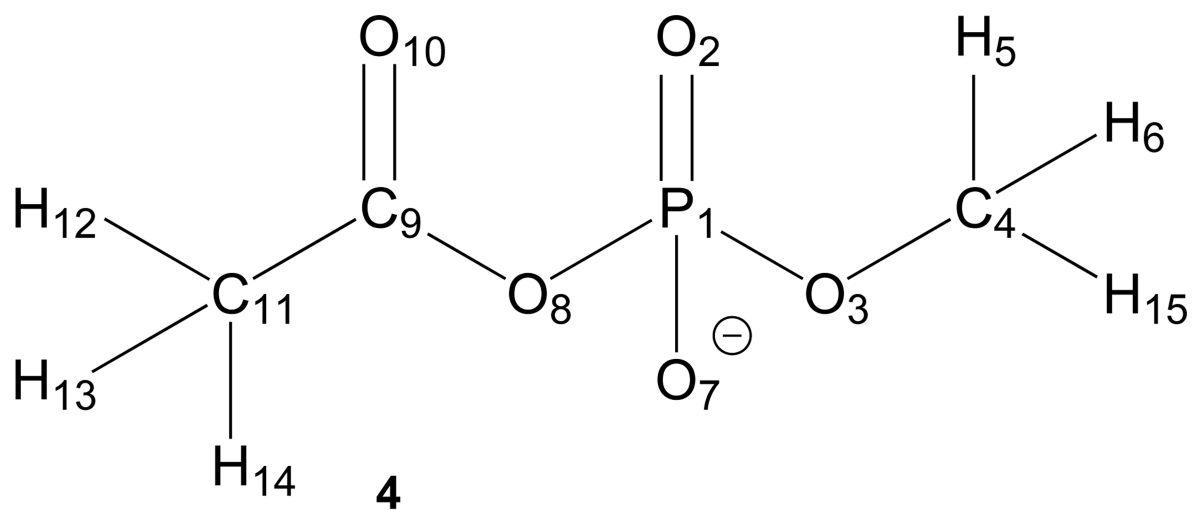
Fig. 3.
Schematic representation of model compounds **4** and **5** showing atom numbering.
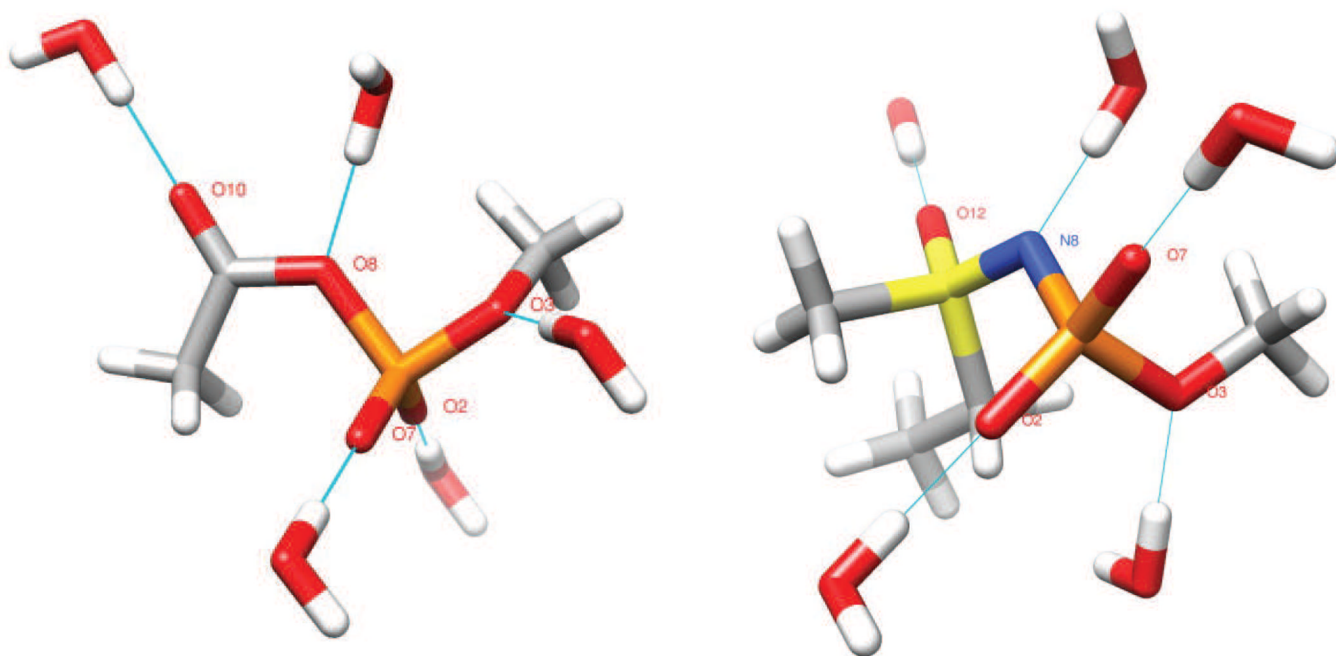
Fig. 4.
Orientations of water molecules about the model compounds **4** (left) and **5** (right) used in atomic partial charge optimization. Note that only a single water molecule is hydrogen bonded to the model structure during each calculation; all waters are shown here merely for convenience. Atom coloring scheme: C, grey; H, white; N, blue; O, red; P, orange; S, yellow.
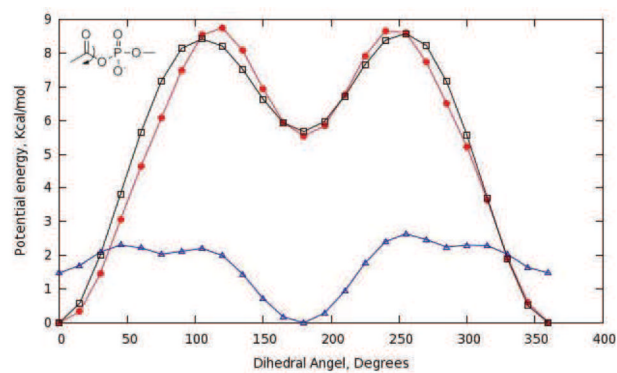
(A) P1-O8-O9-C11 PES
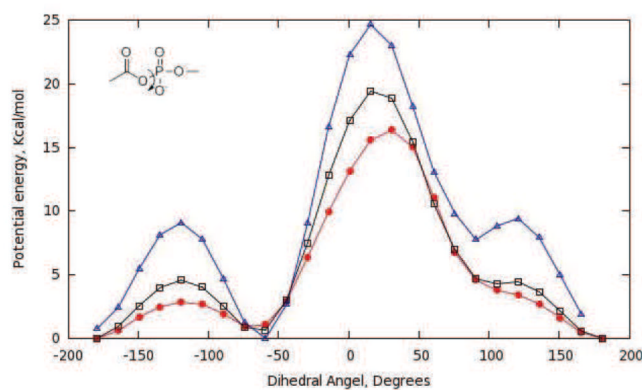
(B) O3-P1-O8-C9 PES
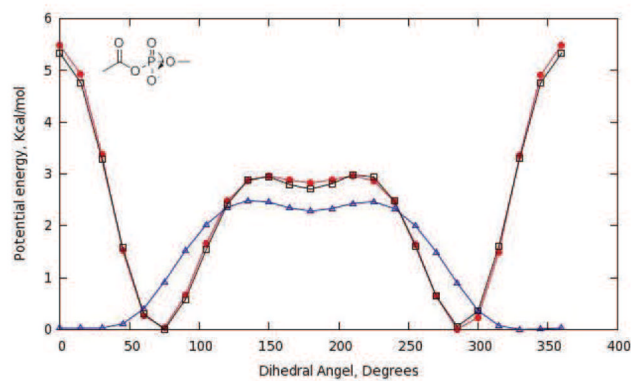
(C) C4-O3-P1-O8 PES

Fig. 5.
Potential energy scans (PES) for optimized dihedral angle parameters in model acylphosphate **4**. QM PES (red), optimized (black) and initial (blue) MM PES. Interaction labels correspond to the atom numbers in Fig. 3.

(A) P1-N8-S11-C13 PES

(B) C19-C9-S11-N8 PES
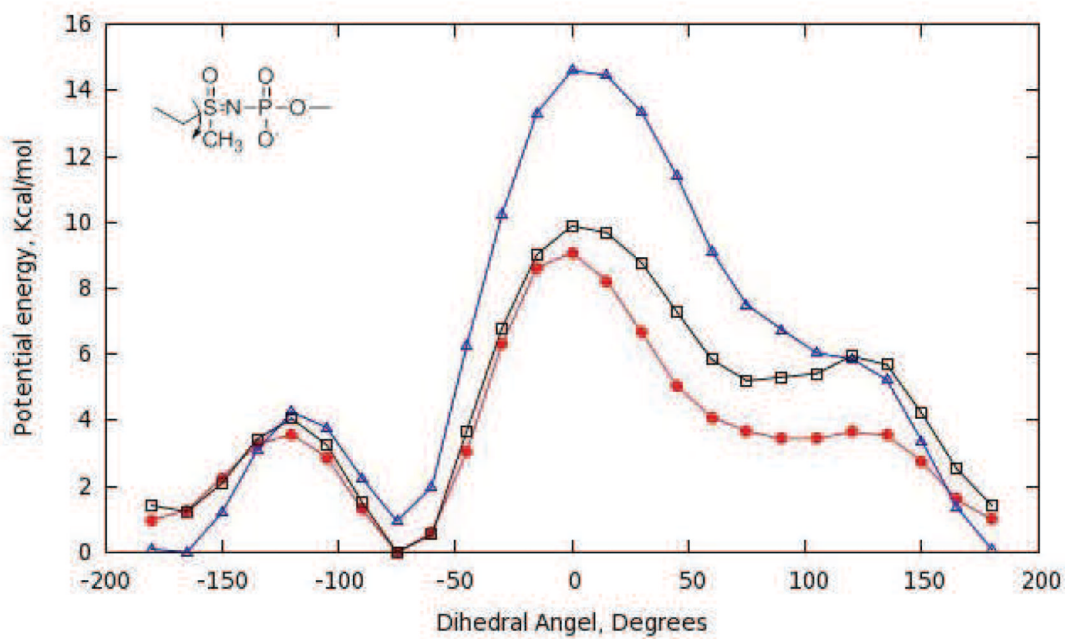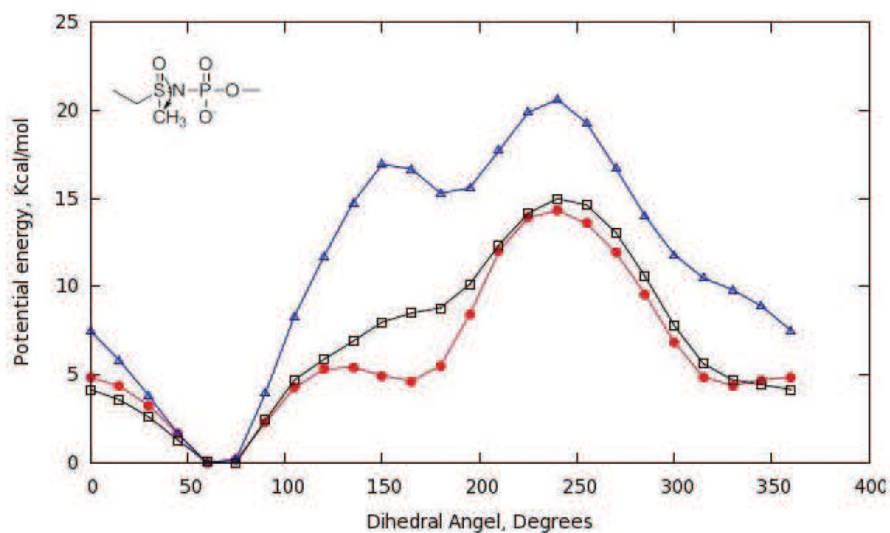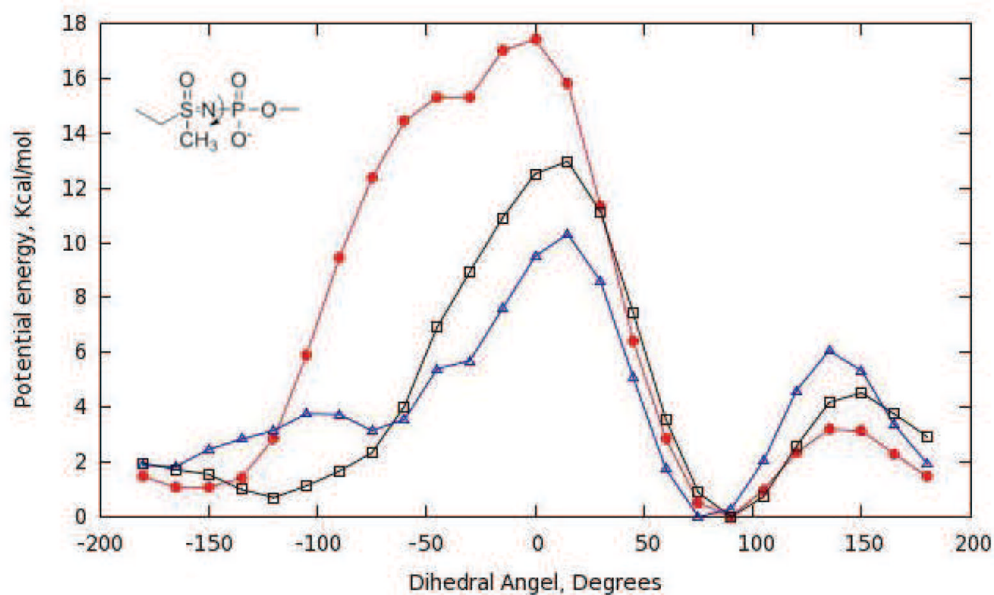
S11-N8-P1-O3 PES
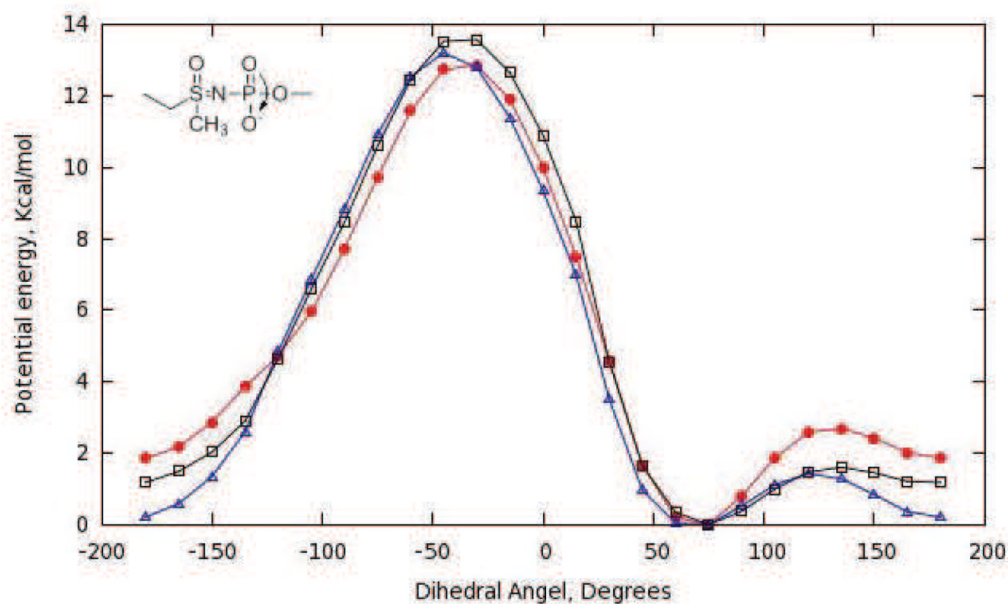
N8-P1-O3-C4 PES

Fig. 6.
Potential energy scans (PES) for optimized dihedral angle parameters in model sulfoximine
5. QM PES (red), optimized (black) and initial (blue) MM PES. Interaction labels
correspond to the atom numbers in Fig. 3.
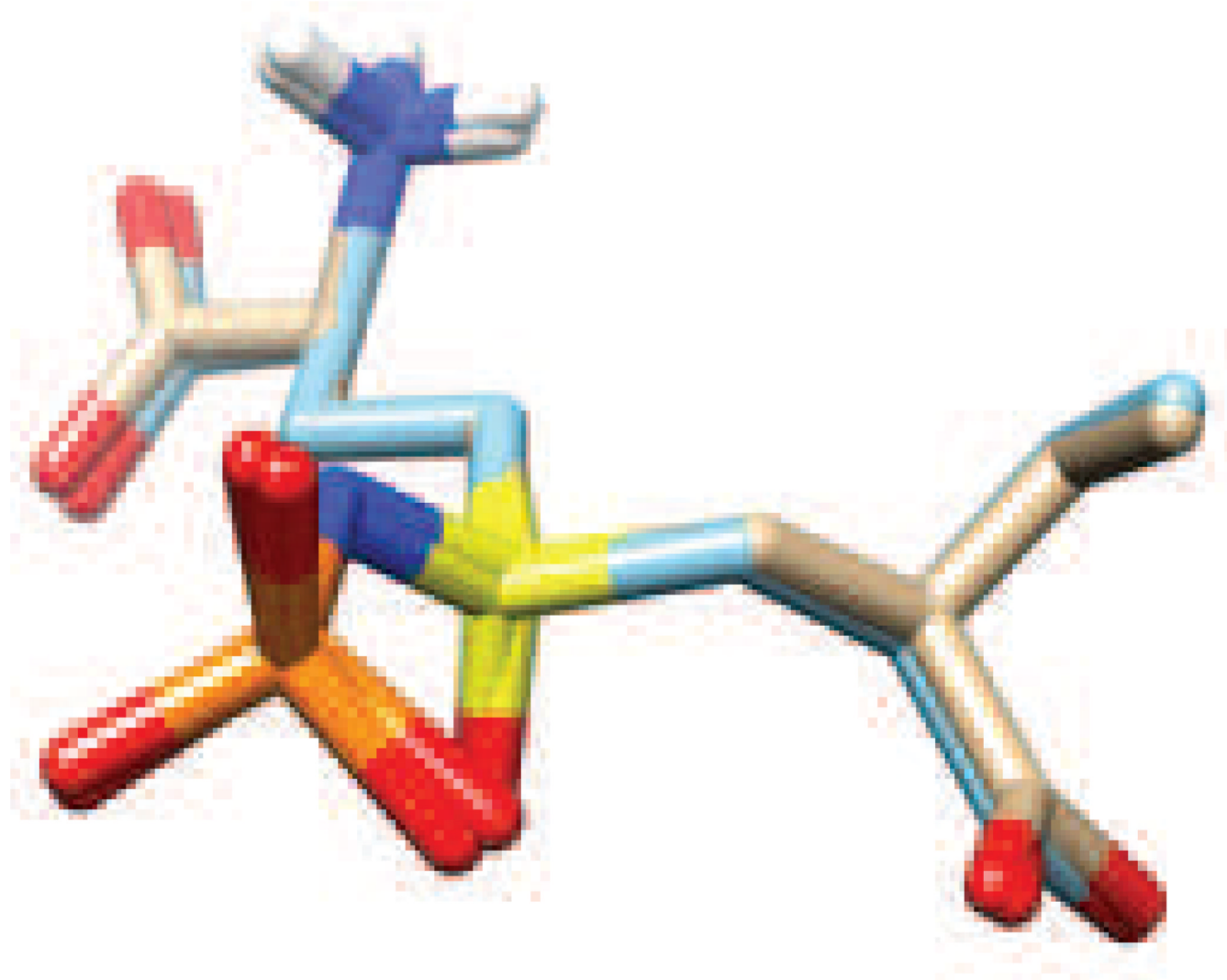
Fig. 7.
Superimposition (RMSD 0.2Å) of the N-phosphorylsulfoximine derivative **6** before (C, brown) and after (C, light blue) energy minimization of the complex of **6** bound to the enzyme γ-glutamylcysteine synthetase. Atom coloring scheme: H, white; N, blue; O, red; S, yellow; P, orange.

(A) O2-P1-O8-C9

(B) O3-P1-O8-C9

(C) O7-P1-O8-C9
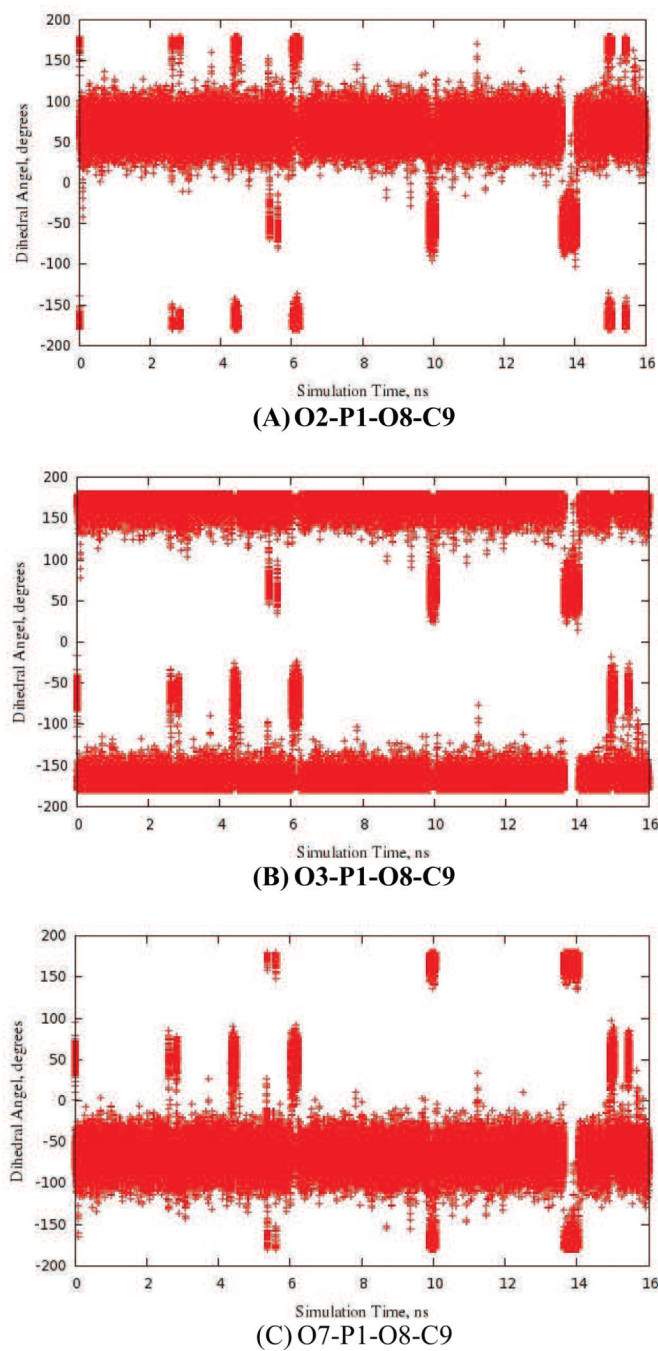
Fig. 8.
MD trajectory data (16 ns) showing that the phosphate moiety in the model acylphosphate **4** undergoes rotation during the simulation. Dihedral angles are labeled with the atom numbers shown in Fig. 3.

Table 1

Optimized atomic partial charges for atoms in the model structures **4** and **5**

	Acylphosphate **4**			N-Phosphonosulfonimidate **5**		
Atom	Type	Charge		Atom	Type	Charge
P1	PG1	1.30		P1	PG1	0.20
O2	OG2P1	−0.71		O2	OG2P1	−0.46
O3	OG303	−0.46		O3	OG303	−0.28
C4	CG331	−0.17		C4	CG331	−0.17
H5	HGA3	0.09		H5	HGA3	0.09
H6	HGA3	0.09		H6	HGA3	0.09
O7	OG2P1	−0.71		O7	OG2P1	−0.46
O8	OG305	−0.38		N8	NG2D1	−0.38
C9	CG2O2	0.34		C9	CG321	0.02
O10	OG2D1	−0.48		H10	HGA3	0.09
C11	CG331	−0.27		S11	SG3O2	0.12
H12	HGA3	0.09		O12	OG2P1	−0.42
H13	HGA3	0.09		C13	CG331	0.11
H14	HGA3	0.09		H14	HGA3	0.09
H15	HGA3	0.09		H15	HGA3	0.09
				H16	HGA3	0.09
				H17	HGA2	0.09
				H18	HGA2	0.09
				C19	CG331	−0.27
				H20	HGA3	0.09
				H21	HGA3	0.09
				H22	HGA3	0.09

Table 2

Interaction energies (kcal/mol) and distances (Å) of water complexed with acylphosphate **4** and N-phosphonosulfonimidoyl derivative **5** in different geometries (see Fig. 4)[a]

Interaction geometry	ΔE (HF)	ΔE (CGenFF)	ΔΔE	r (HF)	r (CGenFF)	Δr
Acylphosphate **4**						
O2...HOH	−11.4	−11.5	−0.1	1.89	1.70	−0.19
O7...HOH	−11.8	−11.5	0.3	1.89	1.70	−0.19
O3...HOH	−7.8	−7.8	0.0	2.03	1.77	−0.26
O8...HOH	−7.7	−7.9	−0.2	2.18	1.91	−0.27
O10...HOH	−8.3	−8.5	−0.2	1.96	1.76	−0.20
AD[b]			−0.05			−0.22
RMSD[b]			0.21			0.05
AAD[b]			0.18			0.22
Phosphonosulfonimidate **5**						
O2...HOH	−13.0	−12.8	0.2	1.83	1.71	−0.12
O7...HOH	−10.0	−11.3	−1.3	1.87	1.73	−0.14
O3...HOH(tet)[c]	−10.0	−10.80	−0.8	1.95	1.76	−0.19
N8...HOH	−10.0	−10.1	−0.1	2.07	1.99	−0.08
O12...HOH	−7.8	−8.0	−0.2	1.98	1.77	−0.21
AD			−0.44			−0.15
RMSD			0.53			0.04
AAD			0.52			0.15

[a] Interaction energies were not scaled as both model compounds are anionic. All HF distances are also reported as their unscaled values; we note, however, that bulk hydrogen bonds are approximately 0.2 Å shorter than in vacuum.

[b] AD, average deviation; RMSD, root mean square deviation; AAD, absolute average deviation.

[c] The interaction between O3 and the water molecule was also modeled in a trigonel geometry (Figure 4): ΔE (HF) −9.9 kcal/mol, ΔE (CGenFF) −8.2 kcal/mol; r (HF) 2.02 Å, r (CGenFF) 1.81 Å. In general, the interaction energies and optimized distances between water molecules and oxygen atoms were modeled in a variety of geometries and all values used to develop the atomic partial charges. Only representative values are included here for clarity.

Table 3

CGenFF- and MP2-Optimized Geometry of Model Compounds **4** and **5**.

Coordinate	MP2	CGenFF	Difference	Coordinate	MP2	CGenFF	Difference
Bond Lengths (Å)				**Angles (°)**			
Acylphosphate **4**							
P1-O8	1.75	1.75	0.00	O3-P1-O8	94	94	0
O8-O9	1.34	1.34	0.00	O2-P1-O8	106	108	2
				O7-P1-O8	108	108	0
Dihedrals (°)				O8-C9-O10	120	120	0
P1-O8-C9-C11	2	2	0				
P1-O8-C9-O10	−178	−178	0				
O2-P1-O8-C9	68	66	−2				
O7-P1-O8-C9	−68	−68	0				
O3-P1-O8-C9	179	177	−2				
O8-P1-O3-C4	−69	−71	−2				
Improper Torsions (°)							
C9-C11-O10-O8	−0.1	0.0	0.1				
Bond Lengths (Å)				**Angles (°)**			
Phosphonosulfonimidate **5**							
P1-N8	1.75	1.75	0.00	O3-P1-N8	100	100	0
N8-S11	1.53	1.53	0.00	O2-P1-N8	109	111	2
				O7-P1-N8	108	107	−1
				C9-S11-N8	112	112	0
				P1-N8-S11	120	120	0
				N8-S11-C13	111	111	0
				N8-S11-O12	116	116	0
Dihedrals (°)							
N8-S11-C9-C19	−176	−169	7				
O2-P1-N8-S11	−24	−23	1				
O7-P1-N8-S11	−161	−155	6				
O3-P1-N8-S11	85	90	5				
P1-N8-S11-C9	−49	−48	0				

Coordinate	MP2	CGenFF	Difference	Coordinate	MP2	CGenFF	Difference
P1-N8-S11-O12	−171	−171	0				
P1-N8-S11-C9	−49	−48	1				
P1-N8-S11-C13	67	67	0				
N8-P1-O3-C4	71	74	3				

Table 4

Vibrational spectra computed for acylphosphate **4** at the scaled MP2 level and with CGenFF[a]

MP2/6-31G(d) scaled by a factor 0.943					CGenFF			
Freq[b]	Assign (%)	Assign (%)	Assign (%)	Assign (%)	Freq[b]	Assign (%)	Assign (%)	Assign (%)
67.0	tdOPOC (98)				68.2	tdCCOP (65)	tdOPOC(29)	
81.8	tdCCOP (73)	tdCOPO (23)			79.8	tdCOPO (47)	tdOPOC (36)	
100.5	tdCOPO (55)	tdCCOP (33)			106.5	tdOPOC (33)	tdCOPO (32)	tdCCOP (23)
140.2	tdPOCH (69)	dPOC9 (14)	scPO4' (9)		141.2	tdPOCH (57)	scPO4' (31)	dPOC9 (8)
180.2	dPOC9 (53)	tdPOCH (24)	scPO4' (11)		207.9	tdPOCH (29)	dPOC9 (18)	rPO4 (16)
194.3	tdPOCH (89)	tdCOPO (12)			239.4	dPOC4 (33)	dPOC9 (19)	rPO4 (14)
219.0	dPOC4 (41)	twPO4 (18)	scPO4' (8)		268.0	tdPOCH (90)		
295.4	scPO4' (38)	twPO4 (20)	dCCO (12)		289.4	dPOC4 (31)	scPO4' (19)	twPO4 (9)
329.7	twPO4 (36)	dPOC4 (19)	saOP (12)		323.4	dCCO (28)	twPO4 (24)	dPOC9 (21)
343.8	dCCO (19)	ssOP (17)	saOP (16)		334.8	twPO4 (38)	wPO4 (28)	dCCO (9)
414.2	scPO4 (42)	wPO4 (20)	rPO4 (11)		417.2	ssOP (30)	scPO4 (24)	rPO4 (20)
460.0	wPO4 (32)	dCCO (24)	rC=O (15)		471.9	wPO4 (36)	dPOC4 (19)	twPO4 (14)
505.7	scPO4 (21)	wPO4 (16)	dPOC4 (15)		499.9	scPO4 (44)	dCCO (27)	dPOC9 (6)
515.2	rPO4 (54)	scPO4 (13)	ssOP (10)		537.0	rC=O (39)	saOP (12)	scPO4 (11)
564.4	tiOCOC (79)	rCH3-C11 (14)			564.3	tiOCOC (90)		
685.5	sCC (34)	rC=O (25)	saOP (16)		671.9	saOP (47)	ssOP (11)	rPO4 (9)
723.7	saOP (38)	ssOP (32)	sO3C (9)		679.6	ssCC (34)	ssOP (18)	rC=O (11)
906.9	sCC (33)	sO8C (26)	rC=O (11)		952.4	sO8C (34)	ssPO (16)	r'CH3C11 (11)
993.8	r'CH3C11 (38)	ssPO (18)	rCH3C11 (13)		996.4	r'CH3C11 (35)	ssPO (34)	rCH3C11 (10)
1035.2	sO3C (59)	ssPO (25)	r'CH3C11 (10)		1023.3	sO3C (23)	ssPO (18)	r'CH3C11 (13)
1043.3	rCH3C11 (53)	r'CH3C11 (20)	tiOCOC (20)		1040.1	sO3C (54)	ssPO (16)	ssOP (8)
1048.6	ssPO (46)	sO3C (27)	ssOP (9)		1046.7	rCH3C11 (64)	r'CH3C11 (19)	ad'CH3C11(10)
1135.9	rCH3C4 (72)	r'CH3C4 (25)			1139.0	rCH3C4 (40)	r'CH3C4 (37)	ad'CH3C4 (19)
1157.5	r'CH3C4 (66)	rCH3C4 (24)			1144.8	r'CH3C4 (39)	rCH3C4 (34)	adCH3C4 (24)
1243.9	saPO (93)				1187.6	saPO (92)	wPO4 (6)	
1258.8	sO8C (45)	sCC (13)	rC=O (12)		1232.3	sO8C (33)	sCC (30)	
1373.0	sdCH3C11 (86)	sCC (8)	sO8C (5)		1387.2	sdCH3C11 (98)	rC=O (23)	

MP2/6-31G(d) scaled by a factor 0.943				CGenFF				
Freq[b]	Assign (%)	Assign (%)	Assign (%)	Freq[b]	Assign (%)	Assign (%)	Assign (%)	Assign (%)
1421.8	sdCH3C4 (99)			1429.7	ad'CH3C4 (58)	adCH3C4 (23)	r'CH3C4 (15)	
1447.1	ad'CH3C4 (92)	rCH3C11 (6)		1434.3	adCH3C11 (91)	rCH3C11 (8)		
1460.0	adCH3C11 (91)			1451.9	ad'CH3C11(88)	rCH3C11 (8)		
1465.0	ad'CH3C4 (92)	ad'CH3C4 (34)		1469.4	adCH3C4 (52)	ad'CH3C4 (21)	rCH3C4 (21)	
1488.9	adCH3C4 (59)	adCH3C4 (36)		1615.8	sdCH3C4 (88)	sO3C (11)		
1673.5	sC=O (84)			1741.2	sC=O (88)	sCC (5)		
2914.5	ssCH3C4 (100)			2854.1	ssCH3C4 (100)			
2936.5	ssCH3C11(100)			2913.1	saCH3C4 (71)	saCH3C4 (29)		
3001.6	saCH3C4 (99)			2915.8	ssCH3C11(100)			
3012.5	saCH3C4 (99)			2917.3	saCH3C4 (71)	saCH3'C4 (29)		
3023.1	saCH3C11 (76)	ssCH3C11 (24)		2973.4	ssCH3C11 (75)	saCH3C11 (25)		
3041.8	ssCH3C11 (76)	saCH3C11 (24)		2975.9	saCH3C11 (75)	ssCH3C11 (25)		

[a]Optimized vibrational contributions from interactions for which parameters have been developed in this study are shown in bold font. s stands for bond stretching with the variations ss and sa for symmetric and asymmetric stretching, respectively. d means angle deformation with the variations sd and ad for symmetric and asymmetric deformation, respectively. td and ti stand for torsional and improper torsion deformation, respectively. sc stands for scissoring, r for rocking, w for wagging and tw for twisting.

[b]Frequencies are expressed in units of cm^{-1}.

Table 5

New bonded interaction parameters assigned for the acylphosphate moiety in **4**

Bonds	Atom Types	R_{eq} [a]	K_R	
P1-O8	PG1-OG305	1.78	170	
C9-O10	CG2O2-OG305	1.34	230	

Bond Angles	Atom Types	Θ_{eq} [b]	K_Θ	R_{UB}	K_{UB}
P1-O8-C9	PG1-OG305- CG2O2	121.5	70		
O2-P1-O8	OG2P1-PG1-OG305	103.0	60		
O3-P1-O8	OG303-PG1-OG305	90.8	60		
O7-P1-O8	OG2P1-PG1-OG305	103.0	60		
O8-C9-O10	OG305- CG2O2- OG2D1	118.0	70	2.26	160
O10-C9-C11	OG305- CG2O2- CG331	104.0	30	2.33	5

Dihedral Angles	Atom Types	K_ϕ [c]	n	δ
P1-O8-C9-O10	PG1-OG305-CG2O2-OG2D1	1.30	1	180
P1-O8-C9-O10	PG1-OG305-CG2O2-OG2D1	2.60	2	180
P1-O8-C9-C11	PG1-OG305-CG2O2-CG331	3.80	1	180
P1-O8-C9-C11	PG1-OG305-CG2O2-CG331	1.60	2	180
O2-P1-O8-C9	OG2P1-PG1-OG305-CG2O2	0.10	3	0
O3-P1-O8-C9	OG303-PG1-OG305-CG2O2	0.10	2	180
O3-P1-O8-C9	OG303-PG1-OG305-CG2O2	0.10	3	0
C4-O3-P1-O8	CG331-OG303-PG1-OG305	1.47	2	0
C4-O3-P1-O8	CG331-OG303-PG1-OG305	0.70	3	0

Improper Torsion	Atom Types	K_ϕ [d]	Φ_o
O8-O10-C11-C9	OG305-OG2D1-CG331-CG2O2	56	0

[a] R_{eq}, reference bond distance (Å) and K_R, force constant (kcal/mol/Å^2).

[b] Θ_{eq}, reference bond angle (°) and K_Θ, force constant (kcal/mol/rad^2).

[c] K_ϕ, torsional potential (kcal/mol), n and δ, periodicity and phase offset (°) of the torsion, respectively.

[d] K_ϕ, improper dihedral potential (kcal/mol/rad^2) and Φ_O, reference improper dihedral angle (°).

Table 6

New bonded interaction parameters assigned for the N-phosphonosulfonimidoyl functional group in **5**

Bonds	Atom Types	R_{eq}[a]	K_R
P1-N8	PG1-NG2D1	1.72	100
N8-S11	NG2D1-SG3O2	1.53	400

Bond Angles	Atom Types	Θ_{eq}[b]	K_Θ
P1-N8-S11	PG1-NG2D1-SG3O2	113.0	30
O2-P1-N8	OG2P1-PG1-NG2D1	106.0	50
O3-P1-N8	NG2D1-PG1-OG303	98.8	94
O7-P1-N8	OG2P1-PG1-NG2D1	106.0	50
N8-S11-C9	NG2D1-SG3O2- CG321	114.3	65
N8-S11-O12	NG2D1-SG3O2- OG2P1	119.0	65
N8-S11-C13	NG2D1-SG3O2- CG321	114.0	79

Dihedral Angles	Atom Types	K_ϕ[c]	n	δ
P1-N8-S11-O2	PG1-NG2D1-SG3O2-OG2P1	2.50	1	180
P1-N8-S11-O2	PG1-NG2D1-SG3O2-OG2P1	1.00	2	0
P1-N8-S11-C9	PG1-NG2D1-SG3O2-CG321	1.00	2	0
P1-N8-S11-C13	PG1-NG2D1-SG3O2-CG331	1.00	1	0
P1-N8-S11-C13	PG1-NG2D1-SG3O2-CG331	0.60	2	0
O2-P1-N8-S11	OG2P1-PG1-NG2D1-SG3O2	0.50	4	0
O3-P1-N8-S11	OG303-PG1-NG2D1-SG3O2	1.80	1	0
O3-P1-N8-S11	OG303-PG1-NG2D1-SG3O2	3.00	2	0
N8-P1-O3-C4	NG2D1-PG1-OG303-CG331	0.40	1	0
N8-P1-O3-C4	NG2D1-PG1-OG303-CG331	0.80	2	0
N8-P1-O3-C4	NG2D1-PG1-OG303-CG331	0.35	3	0
N8-S11-C9-C19	NG2D1-SG3O2-CG321-CG331	1.40	1	180
N8-S11-C9-C19	NG2D1-SG3O2-CG321-CG331	0.001	3	0
N8-S11-C9-H17	NG2D1-SG3O2-CG321-HGA2	0.16	3	0
N8-S11-C13-H14	NG2D1- SG3O2-CG331-HGA3	0.18	3	0

[a] R_{eq}, reference bond distance (Å) and K_R, force constant (kcal/mol/Å^2).

[b] Θ_{eq}, reference bond angle (°) and K_Θ, force constant (kcal/mol/rad^2).

[a] K_ϕ, torsional potential (kcal/mol/rad^2), n and δ, periodicity and phase offset (°) of the torsion, respectively.